

Simulations of Radioactive Decays: an Application of Low-Energy Electromagnetic Packages for the Nuclear Medicine

Munkhbaatar Batmunkh^{1,2,*}, Oleg V. Belov¹, Oidov Lhagva², Lkhagvaa Bayarchimeg¹, Minjgee Minjmaa³ and Purev Battogtokh²

¹Laboratory of Radiation Biology, Joint Institute for Nuclear Research, Joliot-Curie street 6, 141980 Dubna, Moscow region, Russia

²Division of Natural Sciences, National University of Mongolia, University street 1, 210646 Ulaanbaatar, Mongolia

³Department of Radiation oncology, National Cancer Center, Nam Yan Ju Str, Bayanzurkh district, 210648 Ulaanbaatar, Mongolia

Abstract

Key words: Medical radionuclides, *Geant4*, stochastic energy depositions, DNA damage

Article information:
Received: 18 Apr. 2014
Accepted: 07 Dec. 2015
Published: 11 Dec. 2015

Correspondence*:
batmunkh@jinr.ru

Cite this paper as:

Problems of the radiobiology and the nuclear medicine require clarifying the specifics of radionuclides interactions with unhealthy cells. In this work we aimed to simulate emitting particles tracks of radionuclides and their radioactive decays at DNA level inside the cell nucleus. Accordingly, using the Monte Carlo-based track structure simulation technique, we estimated the radial distribution of deposited energy and kinetic energy spectra of electrons produced by primary particles resulting from radioactive decays of different radionuclides within cell nucleus. To address the possibility of DNA damage, we performed the cluster analysis of track structures of emitted particles inside the volumes corresponding to the size of the native double-stranded DNA. For this purpose, *G4-RadioactiveDecay* and low-energy electromagnetic packages from *Geant4* Monte-Carlo toolkit were combined together. Besides, a comparative analysis was performed for various low-energy electromagnetic packages as *G4-DNA* and *G4-Livermore*.

Batmunkh, M., Belov, O. V., Lhagva, O., Bayarchimeg, L., Minjmaa, L. & Battogtokh, P. 2015. Simulations of radioactive decays: an application of low-energy electromagnetic packages for the nuclear medicine. *Mong. J. Biol. Sci.*, 13(1-2): 55-64.

Introduction

Radiation interaction with tissues and track structure of particles in various kinds of substances are found with wide applications in radiotherapy of brain tumors, radiation protection, nuclear physics and space radiobiology. Motivated primarily by the interest to use the radionuclide emissions in the treatment (or to kill) of tumors (thyroid carcinoma, metastatic tumors) and directly killing the sparing cells. Nowadays Monte Carlo simulations has turned out to be useful and common applicable in utilizing and developing

for medical physics and nuclear medicine systems (Amato *et al.*, 2013; Campos, 2008; Buscombe, 2007). In particular, these estimations can be important in two-step targeting which becomes a promising approach in cancer treatment enabling to deliver the toxic substance to the nucleus of the cell (Fondell, 2011). In this regard, simulation of the energy deposition from radionuclides transmitted inside the cell nucleus is required for the correct estimation of DNA damage resulting from nuclide decay.

In this work, we simulated the decays of Iodine (^{125}I) and Bismuth (^{213}Bi) radionuclides distribution inside the spherical model of the cell nucleus. For this purpose, we integrated *G4-DNA* low-energy electromagnetic package with the *G4-RadioactiveDecay* model at nuclear level and which are both fully included in *Geant4* toolkit (Agostinelli *et al.*, 2003; Allison *et al.* 2006). The radionuclide ^{125}I is mainly used for treating thyroid cancer and imaging the thyroid at higher abundance (Li, 2001, 2002; Booz *et al.*, 1987; Toncrova, 2005). ^{125}I with the half-life of 59.4 days emits electron and photons producing the daughter ^{125}Te (Tellurium) nuclide with the energy of 35.4 keV. Since ^{125}Te is an excited state possessing the half-life of 1.6×10^{-9} seconds, it undergoes further decay proceeding to the stable state of nonradioactive ^{125}Te nuclide with zero energy. This transition is characterized by 7% of gamma emission and 93% of internal conversion. An example of ^{125}I radioactive decay is shown in Fig. 1a. The second radionuclide ^{213}Bi is a radioisotope also commonly used for nuclear medicine. In fact, it is used in radioimmunology to treat patients with leukemia, lymphomas, as well as for micrometastatic carcinomas (Dadachova, 2008). It has unique nuclear properties such as a short 45 minutes half-life and high energy (around 8.4 MeV) alpha-particle emission with a high linear energy transfer. A scheme of the ^{213}Bi radionuclide decay is shown in Fig. 1b. In this decay chain, ^{213}Bi (83 protons, 130 neutrons) disintegrates about 98 % by 444 keV electron (beta-minus) emission resulting in ^{213}Po (84 protons, 129 neutrons) and about 2 % through the alpha decay with energy of 5.9 MeV resulting in ^{209}Tl (81 protons, 128

neutrons). The daughter ^{213}Po and ^{209}Tl nuclides are the excited states with the half-life of $4.2 \mu\text{s}$ and 2.2 min. At the next step these nuclides transform to the unstable ^{209}Pb (82 protons, 127 neutrons) by alpha and beta emission with energies of 8.4 MeV and 659 keV respectively. Finally ^{209}Pb decays to the nonradioactive stable ^{209}Bi (83 protons, 126 neutrons) by emission of 198 keV beta particles.

Materials and Methods

Simulation of the radioactive decays. Radioactive decay is a stochastic physics process where an atom with unstable nuclei transmutes into daughter nuclides of loses or gains a neutron or a proton by emitting particles of ionizing radiation. This physics processes does not require external interactions for radioactive decays schemes mentioned in Figure 1.

Monte-Carlo-based technique for simulation of radioactive decay is available in the extended example named *rdecay01* of *Geant4* toolkit. It is based on data taken from Evaluated Nuclear Structure Data File (ENSDF) (Tuli, 1996). This example demonstrates the use of some basic features of *G4-RadioactiveDecay* hadronic package which allows displaying counts of created particles, their kinetic energies, time of life, and activity of individual decays (Truscott *et al.*, 2000).

In the present study, we have adapted low-energy electromagnetic process and a simple spherical model of the tumor cell nucleus with the diameter of $1 \mu\text{m}$ to this *Geant4* code. The radionuclides were placed in the center of cell nucleus.

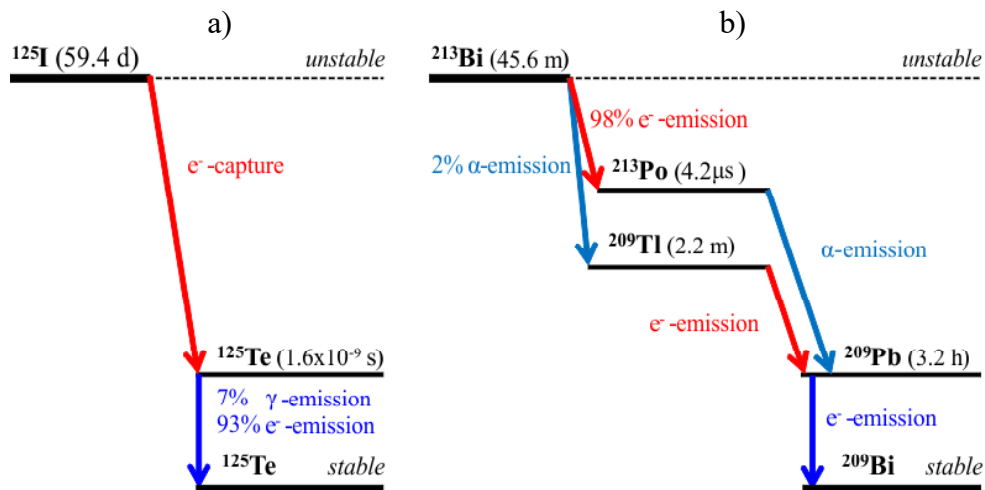


Figure 1. Radioactive decay schemes of the ^{125}I (panel a) and the ^{213}Bi (panel b) radionuclides.

Track structure calculations and cluster analysis. The track structures of particles emitted in ^{125}I and ^{213}Bi radioactive decays are calculated by the *G4-DNA* and *G4-Livermore* low-energy electromagnetic packages assuming the random distribution of the particles inside the cell nucleus. The *G4-DNA* package is an extension of standard *Geant4* toolkit for simulating the physical and radiobiological processes at cellular and nanometer scales (Agostinelli *et al.*, 2003; Allison *et al.*, 2006).

The physics of atomic interaction are characterized by the processes of ionization, excitation (electronic and vibrational), molecular attachment and elastic scattering for emitted electrons and photons. Ionization, excitation, and charge transfer were taken into account for emitted protons and alpha particles. Decays of both radionuclides are simulated with lower cut off energies of 7.4 eV for electrons. Besides, *G4-Livermore* package: photo-electric effect, Compton and Rayleigh scattering, gamma conversion for photons, ionization, multiple scattering for electrons and positrons, and production threshold value of low energy emission down to 250 eV.

In our simulation code, spatial energy depositions of stochastic traveling emitted particles are defined in the points with coordinates corresponding to each particle interaction in the cell nucleus. This allows estimating the distribution of energy depositions along the radius of nucleus as well as the energy spectrum of emitted particles and distribution of the specific energy (i.e., dose deposit). The specific energy z which is also sometimes called deposited dose in

cell nucleus can be calculated by $z = \varepsilon_i / \rho V$, where ε_i is the energy imparted defined by the sum of all energy depositions to nucleus solid in a given volume caused by a single event (ICRU Report 86, 2011). In our calculations, ρ is the density of liquid water equaling to 1 g cm^{-3} and V is the volume of spherical model representing the cell nucleus ($V = 4.18 \mu\text{m}^3$).

To address the possibility of DNA damage, we also performed the cluster analysis of track structures of emitted particles at nanometer scale. For this purpose we used the cluster analyzing algorithm developed earlier (Batmunkh *et al.*, 2013). The diameter of all produced clusters was set to be 2 nm that corresponds to the diameter of the native double-stranded DNA. This enables estimating the frequency distribution of particles affecting DNA and calculating the number of DNA segments hit by particles.

Results and Discussion

Track structures of radioactive decays.

For estimation of quantities referred to energy deposition, we simulated track structures of 1000 decays from each of ^{125}I and ^{213}Bi radionuclides. An example of ^{125}I radionuclide decay simulations for the lesser number of events equaling to 10 is shown in Fig. 2. Here, both low-energy electromagnetic packages *G4-DNA* and *G4-Livermore* were compared for track structures decays of emitted particles products from a radionuclide. The depicted 10-event track structures are characterized by the numerical results presented in Tables 1–3. The parameters

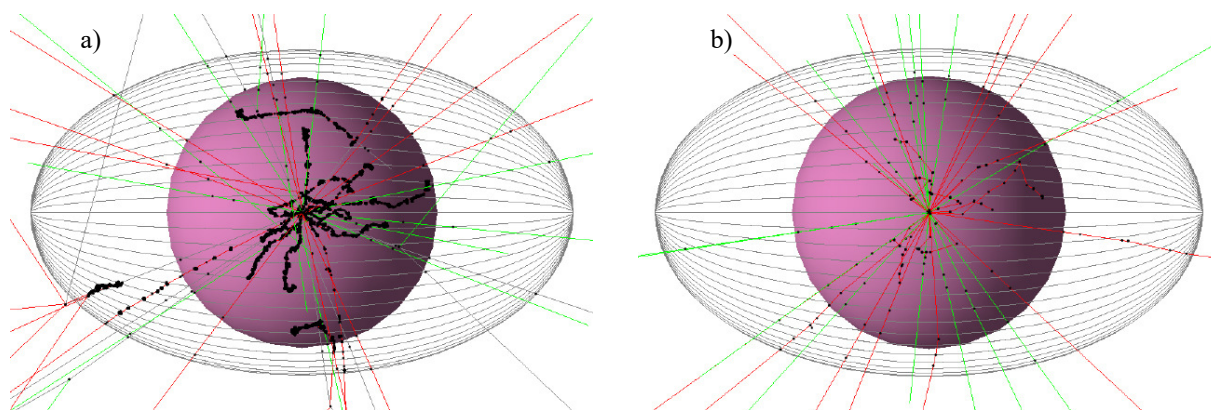


Figure 2. The track structures of emitted particles from radioactive decays of 10 events for radionuclide ^{125}I . These estimations are performed using the both low-energy electromagnetic packages of *G4-DNA* (panel a) and *G4-Livermore* (panel b). The cell nucleus is computed as violet spherical solid with $1 \mu\text{m}$ diameter and nuclear membrane is represented as gray-line connected elliptical volume. The red and green line is emitted electrons and photons. Track structures of energy depositions within and outside cell nucleus were simulated down to the nanometer scale and that's represented as black dots.

Table 1. The number of emitted particles generated during calculations and their mean energy.

Type of the particle	¹²⁵ I				²¹³ Bi			
	Number of emitted particles		Mean energy of emitted particles (keV)		Number of emitted particles		Mean energy of emitted particles (keV)	
Type of the process	<i>G4-DNA</i>	<i>G4-Livermore</i>	<i>G4-DNA</i>	<i>G4-Livermore</i>	<i>G4-DNA</i>	<i>G4-Livermore</i>	<i>G4-DNA</i>	<i>G4-Livermore</i>
e^-	1694	20	0.056	4.75	28658	358	0.24	19.36
γ	1	1	35.49	35.49	3	6	440.5	658.4
ν_{e^-}	10	10	150.3	150.3	-	-	-	-
$\bar{\nu}_{e^-}$	-	-	-	-	20	20	656.6	624.2
α	-	-	-	-	12	10	8368	8126
α^+	-	-	-	-	2	-	8325	-
He	-	-	-	-	1	-	8365	-

Table 2. The number of physical processes generated by *Geant4* for the emitted particles.

Process name	Number of processes			
	¹²⁵ I		²¹³ Bi	
	<i>G4-DNA</i>	<i>G4-Livermore</i>	<i>G4-DNA</i>	<i>G4-Livermore</i>
<i>RadioactiveDecay</i>	24	27	39	43
<i>Transportation</i>	12	11	77	36
<i>e-_G4DNAIonisation</i>	1685	-	19035	-
<i>e-_G4DNAElastic</i>	86245	-	1245054	-
<i>e-_G4DNAExcitation</i>	225	-	3169	-
<i>e-_G4DNAVibExcitation</i>	9721	-	140212	-
<i>e-_G4DNAAttachment</i>	31	-	437	-
<i>α_G4DNAIonisation</i>	-	-	9571	-
<i>α_G4DNAExcitation</i>	-	-	802	-
<i>α_G4DNAChargeDecrease</i>	-	-	2	-
<i>α+_G4DNAIonisation</i>	-	-	6	-
<i>α+_G4DNAExcitation</i>	-	-	4	-
<i>α+_G4DNAChargeIncrease</i>	-	-	2	-
<i>He_G4DNAIonisation</i>	-	-	-	-
<i>He_G4DNAChargeIncrease</i>	-	-	1	-
<i>He_G4DNAExcitation</i>	-	-	-	-
<i>Photo-electric</i>	-	1	-	4
<i>multiple scattering</i>	-	75	-	1964
<i>eIonisation</i>	-	20	-	177
<i>eBremsstrahlung</i>	-	3	-	22
<i>ionIonisation</i>	-	20	-	372

Table 3. The mean values of deposited energy (\bar{E}), dose deposit (D), and mean specific activity as estimated in calculations. Specific activity is defined as an activity per unit of mass of the primary radionuclide. Activity of radioactive decay is expressed as the number of atoms that decay per unit of time. The value of radioactive decay is expressed here in Ci (Curie) [$1 \text{ Ci} = 3.7 \times 10^{10} \text{ Bq}$].

Parameter	^{125}I		^{213}Bi	
	<i>G4-DNA</i>	<i>G4-Livermore</i>	<i>G4-DNA</i>	<i>G4-Livermore</i>
\bar{E} , keV	2.98 ± 0.96	3.41 ± 1.21	216.22 ± 12.27	218.91 ± 16.34
D , Gy	0.14 ± 0.03	1.13 ± 0.05	8.47 ± 0.04	8.37 ± 0.09
Mean specific activity, Ci/g	2.23×10^4	1.14×10^4	2.65×10^7	2.09×10^7

which were scored include the number of emitted particles and their kinetic energies, counts of physical processes generated during calculations of ^{125}I and ^{213}Bi decays respectively, the mean deposited energy, \bar{E} and the mean dose deposit, D represented as the specific energy z . The numerical results and plots depicting the track structures were obtained with the ROOT object-oriented data analysis framework (Brun *et al.*, 1997).

Cluster analysis. Limiting the space by the size of cell nucleus we calculated the frequency distribution of cluster sizes from all particles' track structures. Here the cluster size is considered as the number of ionizations inside the spherical volume equaling to diameter of the native double-stranded DNA. Fig. 3a shows the distributions computed for ^{125}I and ^{213}Bi . These results show that the most probable cluster size for the concerned nuclides equals to 3 ionizations inside.

This is enough to produce more than one complex DNA lesion including double-strand breaks. In this regard, our data is in agreement with findings reviewed in (Elmroth *et al.*, 2005).

Furthermore, the curve obtained for ^{213}Bi has a pronounced plateau indicating the formation of clusters with the higher number of ionizations equaling to ~ 24 – 30 . In contrast with this, ^{125}I demonstrates the different pattern of distribution for cluster sizes greater than 20.

Along with the cluster analysis, we estimated the total energy deposited in produced clusters (Fig. 3b). The plot demonstrates that number of created clusters is directly related to deposited energy in created clusters. Accordingly, decreases energy deposition when increases cluster size, but to compare number of clusters, the broader distributions and highly-localized energy deposition in higher cluster size. In the case of

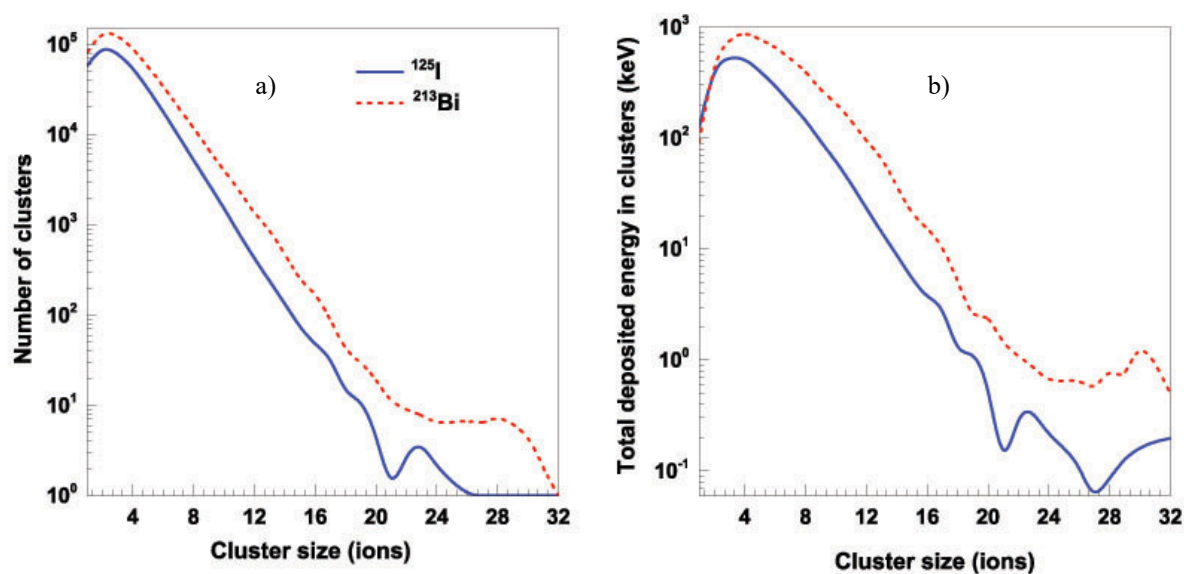


Figure 3. Cluster size distribution (panel *a*) and distribution of total deposited energy deposited to each created cluster (panel *b*) in the case of ^{125}I and ^{213}Bi radionuclides. The cluster diameter is set to be 2 nm.

^{213}Bi , localized energy deposition is lower on 1-2 ionizations in cluster and also higher-broader distributions appearing in cluster size more 3 than for ^{125}I .

As above results, we demonstrated that DNA lesions strongly depends on ionization density of higher charged radionuclides. In Fig. 2, we can see that when enable *G4-DNA*, emitted particles tracks and energy deposits turned out to be distributed more densely than *G4-Livermore*. A comparative analysis of cluster analysis was performed for *G4-DNA* and *G4-Livermore* packages, that shown in Fig. 4. For *G4-DNA* package, cluster size is higher-broader frequently and total deposited energies have broader distribution in comparison to *G4-*

Livermore package. This broader distributions and highly-localized energy depositions for each emitted particle in cell nucleus were directly correlated to complex types of DNA lesions.

For *G4-Livermore*, deposited energy and cluster number are most probable at a cluster of 1 ion, and number of created cluster was fewer. It's produced to be single-strand or base damage of DNA lesions. In fact, emitted particles and energy depositions was distributed very scarcely for *G4-Livermore*. Therefore, track structure simulation at nanometer scale need to enable *G4-DNA* package in furthermore. In contrary, mean energy and dose deposit in cell nucleus were closely equal in the both packages as shown in Table 3.

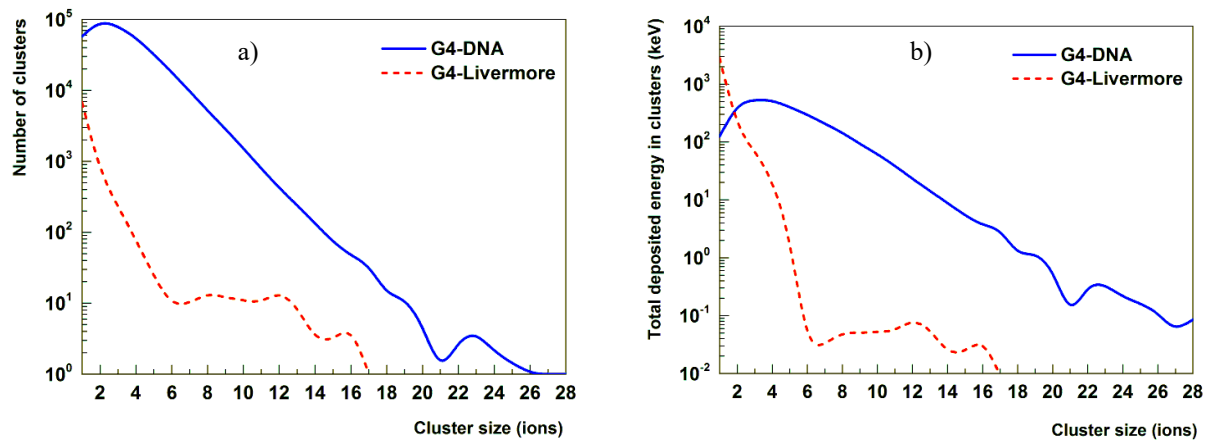


Figure 4. Distributions of cluster size (ions) (panel a) and distribution of total deposited energy of each created cluster (panel b) in the case of ^{125}I radionuclide, emitted particles generated by *G4-DNA* and *G4-Livermore* packages.

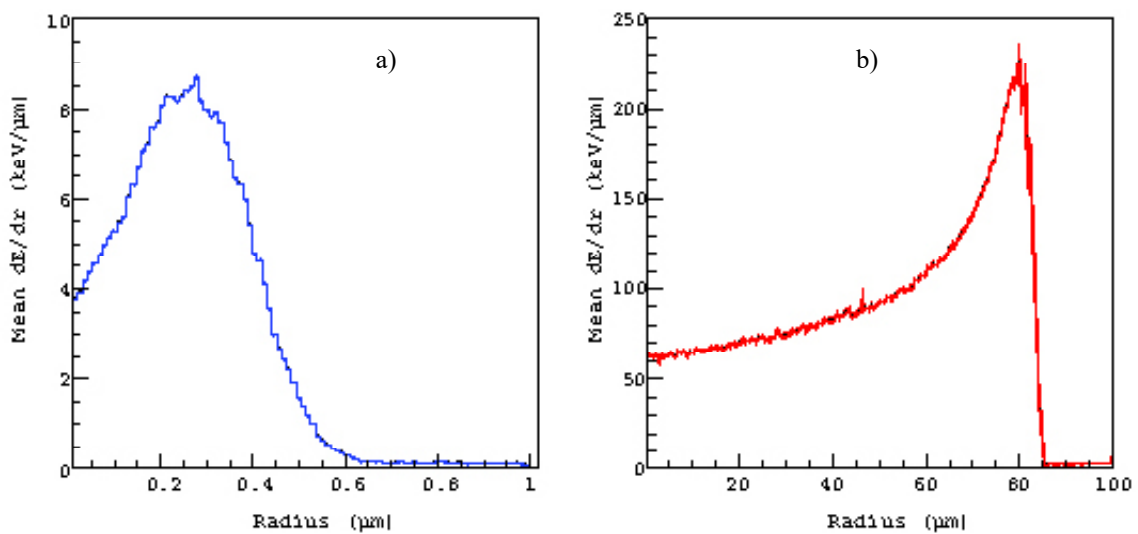


Figure 5. The radial distribution of energy deposited inside the cell nucleus along trajectories of all emitted particles. The results are represented per event of ^{125}I (panel a) and ^{213}Bi (panel b) decay. The radial energy deposition gets more at 0.3 μm in radius for ^{125}I decays, and for ^{213}Bi decay increase in ionization density is seen at the end of emitted particles, which also known as Bragg curve and peak occurs about 80 μm in radius.

Radial distribution of energy deposition.

In our study, we also computed the radial distribution of energy deposited inside the cell nucleus along all trajectories of emitted particles of both radionuclides (Fig. 5). Depicted curves characterize the so-called longitudinal energy profile, or depth dose distribution of emitted particles calculated with the *G4-DNA* package. The comparison of the data obtained for two nuclides shows that ^{125}I delivers the maximal energy at the radius of about $0.3\ \mu\text{m}$ while ^{213}Bi demonstrates a more expanded pattern of energy deposition with the peak within the radius of about $0.3\ \mu\text{m}$. Considering the effect from a single nuclide, these facts suggest that ^{125}I is more convenient to precise killing of individual tumor cells with minimal damage to neighboring ones

whereas ^{213}Bi can be effectively used for micro metastases representing larger objects with the radius of up to $80\ \mu\text{m}$.

Physical characteristics of ^{125}I and ^{213}Bi decays. In this section, we report the comparison of several physical characteristics of decays of two radionuclides. We calculated the total life-time of decay chain per event for both radionuclides (Fig. 6) and estimated the kinetic energy spectrum of primary electrons from 1000 decays of each radionuclide (Fig. 7) and the distribution of spatial energy deposition of portion of their electrons emitted only inside the cell nucleus (Fig. 8). In the case of ^{213}Bi , more electrons of high kinetic and deposited energies are generated, which leads to the shorter life time than for ^{125}I . The results on calculation of the kinetic energy spectrum and the

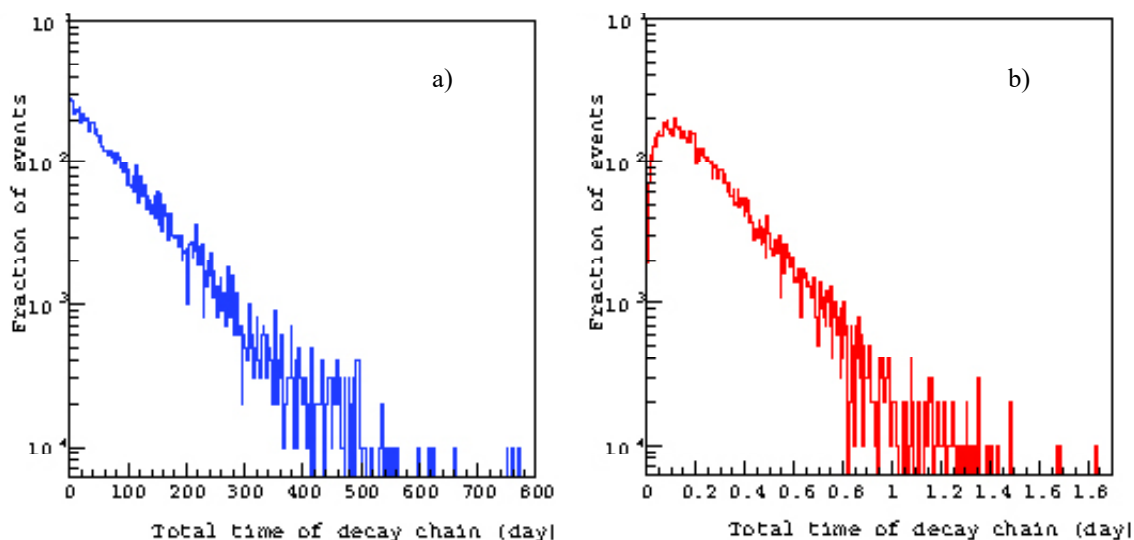


Figure 6. The total life time of decay chain of ^{125}I (panel *a*) and ^{213}Bi (panel *b*) radionuclides.

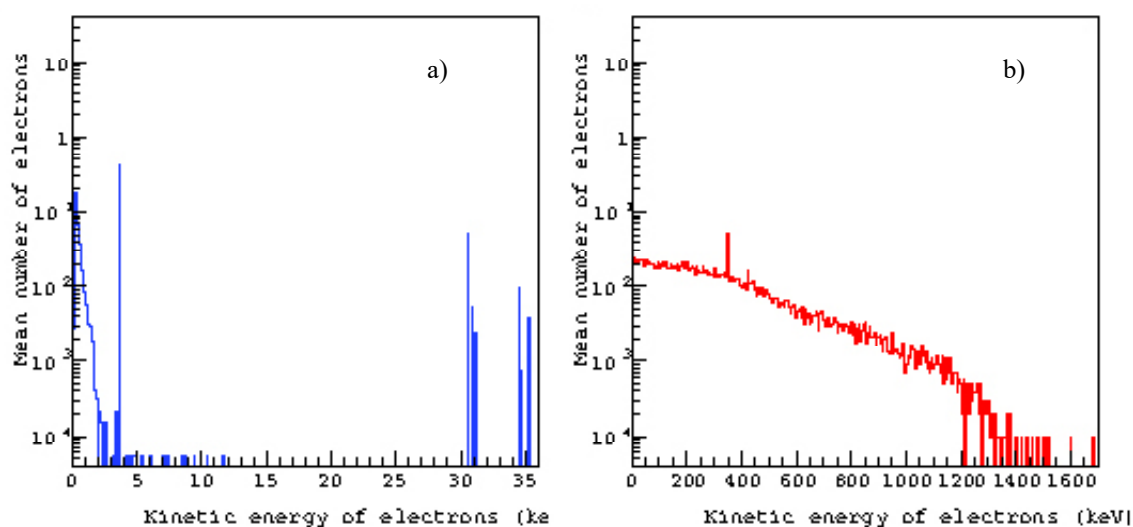


Figure 7. Kinetic energy spectrum of primary electrons per event of ^{125}I (panel *a*) and ^{213}Bi (panel *b*) decay.

total electron energy deposition of ^{125}I decay were compared with Monte Carlo simulations of other authors (Li *et al.*, 2001; Booz *et al.*, 1987).

Our simulations enabled to obtain the spectrum of specific energy in ^{125}I and ^{213}Bi decays inside the cell nucleus (Fig. 9). To estimate the mean specific energy, we applied a Gaussian fit to the computed data. It gave the mean value of 0.14 ± 0.03 Gy for ^{125}I and 8.47 ± 0.04 Gy for ^{213}Bi decay. According to definition of the absorbed dose (ICRU Report 86, 2011) these values can be considered as the dose absorbed inside the cell nucleus. From our estimations it can be also concluded that ^{125}I may deliver smaller dose with lower probability than ^{213}Bi .

Conclusion

We developed the combined package for simulation the track structures of particles emitting from radionuclides placed inside a cell nucleus. The simulation code integrates *G4-RadioactiveDecay* and *G4-DNA* (and also *G4-Livermore*) sub-packages of *Geant4* toolkit (version 9.6). Using this approach, we estimated the spatial distribution of energy deposition from decays of ^{125}I and ^{213}Bi radionuclides placed inside the cell nucleus. In particular, the radial distribution of deposited energy along the radius of cell nucleus was estimated, which is most important for directly tumor cell killing. In our

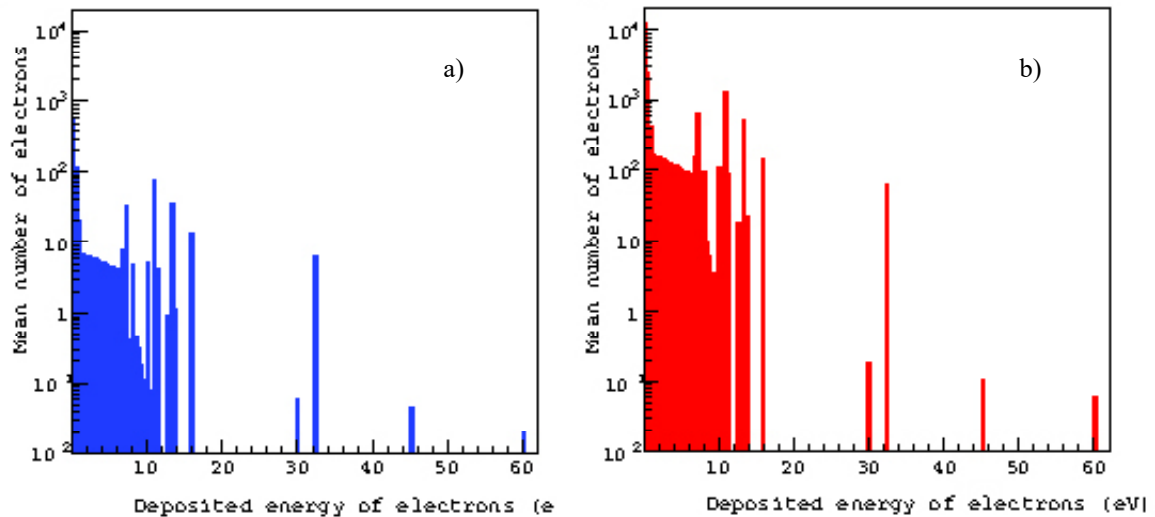


Figure 8. The spatial distribution of energy deposition per event of emitted electron inside the cell nucleus from ^{125}I (panel *a*) and ^{213}Bi (panel *b*) decays.

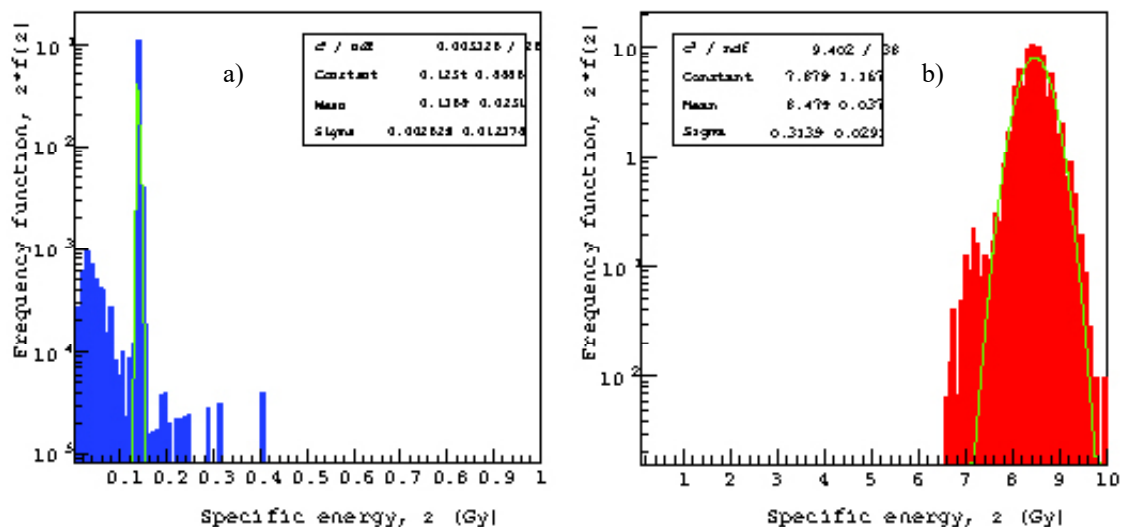


Figure 9. The spectrum of the specific energy per event in the cell nucleus, adjusted to Gaussian distribution. Panel *a* shows the distribution for decay of ^{125}I ; panel *b* represents the distribution for decay ^{213}Bi .

analysis, we also calculated the total life-time of decay chain per decay, kinetic energy spectrum of the emitted electrons and total deposited energy per decay. Our simulations are in the concordance with the data indicating that ^{213}Bi exhibits a shorter time of decay chain than ^{125}I .

In our analysis, we performed the cluster analysis of spatial distribution of energy deposition from particles emitted inside the 1 μm -diameter cell nucleus. In order to address the possibility of DNA damage, we calculated the frequency distribution of emitted particles using the cluster size of 2 nm, which corresponds to the diameter of the native double-stranded DNA helix. Our calculations demonstrate that for ^{213}Bi the probability of ionization inside a cluster is higher than for ^{125}I . ^{213}Bi also exhibits the broader distribution of energy deposition in clusters than ^{125}I . A comparative analysis of cluster analysis was performed for *G4-DNA* and *G4-Livermore* packages. We was illustrated that when enable *G4-DNA*, emitted particles tracks and energy deposits turned out to be distributed more densely and cluster size and total deposited energies per cluster have broader distribution than *G4-Livermore*. As the results, appeared DNA lesions strongly depends on ionization density.

Our study suggests that the package we use may be utilized in solving not only radiation research problems, but it also may have wide applications in educational and practical purposes.

Acknowledgements

The authors would like to thank academician E. A. Krasavin, director of the JINR Laboratory of Radiation Biology and Dr J. Davaasambuu, director of the Department of Science and Technology MECS, Government of Mongolia for their permanent attention and support.

References

- Agostinelli, S., Allison J., Amako K., Apostolakis J., Araujo H., Arce P., Asai M., Axen D., Bannerjee S., Barrand G., Behner F., Bellagamba L., Boudreau J., Broglia L., Brunengo A., Burkhardt H., Chauvie S., Chuma J., Chytraccek R., Cooperman G., Cosmo G., Degtyarenko P., Dell'Acqua A., Depaula G., Dietrich D., Enami R., Feliciello A., Ferguson C., Fesefeldt H., Folger G., Foppiano F., Forti A., Garelli S., Giani S., Giannitrapani R., Gibin D., Gómez Cadenas, J. J., González, I., Gracia Abril, G., Greeniaus, G., Greiner, W., Grichine, V., Grossheim, A., Guatelli, S., Gumplinger, P., Hamatsu, R., Hashimoto, K., Hasui, H., Heikkinen, A., Howard, A., Ivanchenko, V., Johnson, A., Jones, F. W., Kallenbach, J., Kanaya, N., Kawabata, M., Kawabata, Y., Kawaguti, M., Kelner, S., Kent, P., Kimura, A., Kodama, T., Kokoulin, R., Kossov, M., Kurashige, H., Lamanna, E., Lampén, T., Lara, V., Lefebvre, V., Lei, F., Liendl, M., Lockman, W., Longo, F., Magni, S., Maire, M., Medernach, E., Minamimoto, K., Mora de Freitas, P., Morita, Y., Murakami, K., Nagamatu, M., Nartallo, R., Nieminen, P., Nishimura, T., Ohtsubo, K., Okamura, M., O'Neale, S., Oohata, Y., Paech, K., Perl, J., Pfeiffer, A., Pia, M.G., Ranjard, F., Rybin, A., Sadilov, S., Di Salvo, E., Santin, G., Sasaki, T., Savvas, N., Sawada, Y., Scherer, S., Sei, S., Sirotenko, V., Smith, D., Starkov, N., Stoecker, H., Sulkimo, J., Takahata, M., Tanaka, S., Tcherniaev, E., Safai Tehrani, E., Tropeano, M., Truscott, P., Uno, H., Urban, L., Urban, P., Verderi, M., Walkden, A., Wander, W., Weber, H., Wellisch, J. P., Wenaus, T., Williams, D. C., Wright, D., Yamada, T., Yoshida, H. & Zschesche, D. 2003. Geant4 a simulation toolkit. *Nucl. Instr. Meth. A.* 506: 250–303.
- Allison, J., Amako, K., Apostolakis, J., Araujo, H., Dubois, P.A., Asai, M., Barrand, G., Capra, R., Chauvie, S., Chytraccek, R., Cirrone, G.A.P., Cooperman, G., Cosmo, G., Cuttone, G., Daquino, G.G., Donszelmann, M., Dressel, M., Folger, G., Foppiano, F., Generowicz, J., Grichine, V., Guatelli, S., Gumplinger, P., Heikkinen, A., Hrivnacova, I., Howard, A., Incerti, S., Ivanchenko, V., Johnson, T., Jones, F., Koi, T., Kokoulin, R., Kossov, M., Kurashige, H., Lara, V., Larsson, S., Lei, F., Link, O., Longo, F., Maire, M., Mantero, A., Mascialino, B., McLaren, I., Lorenzo, P.M., Minamimoto, K., Murakami, K., Nieminen, P., Pandola, L., Parlati, S., Peralta, L., Perl, J., Pfeiffer, A., Pia, M.G., Ribon, A., Rodrigues, P., Russo, G., Sadilov, S., Santin, G., Sasaki, T., Smith, D., Starkov, N., Tanaka, S., Tcherniaev, E., Tome, B., Trindade, A., Truscott, P., Urban, L., Verderi, M., Walkden, A., Wellisch, J.P., Williams, D.C., Wright, D. & Yoshida, H. 2006. Geant4 developments and applications. *IEEE Trans. Nucl. Sci.*, 53: 270–278.

- Amato, E., Italiano A., Minutoli F. & Baldari S. 2013. Use of the Geant4 Monte Carlo to determine three-dimensional dose factors for radionuclide dosimetry. *Nucl. Instrum. Meth. A.*, 708: 15–18.
- Batmunkh, M., Bayarchimeg, L., Lkhagva, O. & Belov, O. 2013. Cluster Analysis of HZE Particle Tracks as Applied to Space Radiobiology Problems. *Physics of Particles and Nuclei Letters*, 10(7): 854–859.
- Booz, J., Paretzke, H.G, Pomplun, E. & Olko, P. 1987. Auger-electron cascades, charged potential and microdosimetry of Iodine-125. *Radiat. Environ. Biophys.*, 26: 151–162.
- Brun, R. & Rademakers, F. 1997. ROOT – An object oriented data analysis framework. *Nucl. Instrum. Meth. A.*, 389: 81–86.
- Buscombe J.R., 2007. Radionuclides in the management of thyroid cancer. *Cancer Imaging*, 7: 202–209.
- Campos, L. 2008. Dosimetry in thyroid follicles due to low-energy electrons of iodine using the Monte Carlo method. *Radiol. Bras.*, 41: 403–407.
- Dadachova, E. 2008. Radioimmunotherapy of infection with ^{213}Bi -labeled antibodies. *Curr Radiopharm.*, 1: 234–239.
- Elmroth, K. & Stenerlow, B. 2005. DNA-incorporated ^{125}I induces more than one double-strand break per decay in mammalian cells. *Radiat. Res.*, 163: 369–373.
- ICRU Report 86. 2011. Quantification and Reporting of Low-Dose and Other Heterogeneous Exposures. *Journal of the ICRU*. 11(2): 69 pp.
- Fondell, A. 2011. Two-step targeting for effective radionuclide therapy: Preclinical evaluation of ^{125}I -labelled anthracycline delivered by tumour targeting liposomes, Digital Comprehensive Summaries of Uppsala Dissertations from the Faculty of Medicine. Uppsala: *Acta Universitatis Upsaliensis*, 708: 1651–6206.
- Li, W.B., Friedland, W., Pomplun, E., Jacob, P., Paretzke, H. & Lassmann. M. 2001. Track structures and dose distributions from decays of ^{131}I and ^{125}I in and around water spheres simulating micrometastases of differentiated thyroid cancer. *Radiat. Res.*, 156: 419–429.
- Li, W. 2002. Iodine-125 Induced DNA Strand Breakage: Contributions of Different Physical and Chemical Radiation Action Mechanisms. Technische Universität München, Dissertation.
- Toncrova, H. 2005. Simulation of DNA damages induced by incorporated ^{125}I . Czech Technical University in Prague, Dissertation.
- Tuli, J. 1996. *Evaluated nuclear structure data file*, Nucl. Instrum. Meth. A. 369: 506–510.
- Truscott, P., Fan, L., Dyer, C., Ferguson, C., Gurriaran, R., Nieminen, P., Daly, E., Apostolakis, J., Giani, S., Pia, M.G., Urban, L. & Maire, M. 2000. Geant4-a new Monte Carlo toolkit for simulating space radiation shielding and effects, *Radiation Effects Data Workshop. Reno, NV*, pp. 147–152.
